Preparation of decoherence-free cluster states with optical superlattices

Liang Jiang,[1] Ana Maria Rey,[2,3] Oriol Romero-Isart,[4] Juan José García-Ripoll,[5] Anna Sanpera,[4,6] and Mikhail D. Lukin[1,2]

[1]*Department of Physics, Harvard University, Cambridge, Massachusetts 02138, USA*
[2]*Institute for Theoretical Atomic, Molecular and Optical Physics, Cambridge, Massachusetts 02138, USA*
[3]*JILA and Department of Physics, University of Colorado, Boulder, Colorado 80309-0440, USA*
[4]*Departament de Física, Universitat Autònoma de Barcelona, E-08193 Bellaterra, Catalonia, Spain*
[5]*Facultad de CC. Físicas, Universidad Complutense de Madrid, Ciudad Universitaria s/n, Madrid E-28040, Spain*
[6]*Institució Catalana de Recerca i Estudis Avançats, E-08010 Barcelona, Spain*

We present a protocol to prepare decoherence-free cluster states using ultracold atoms loaded in a two dimensional superlattice. The superlattice geometry leads to an array of 2×2 plaquettes, each of them holding four spin-1/2 particles that can be used for encoding a single logical qubit in the twofold singlet subspace, insensitive to uniform magnetic field fluctuations in any direction. Dynamical manipulation of the supperlattice yields distinct inter- and intraplaquette interactions and permits us to realize one qubit and two qubit gates with high fidelity, leading to the generation of universal cluster states for measurement based quantum computation. Our proposal based on inter- and intraplaquette interactions also opens the path to study polymerized Hamiltonians which support ground states describing arbitrary quantum circuits.

I. INTRODUCTION

Quantum technology, in particular quantum information processing and quantum metrology, requires the precise preparation of quantum states that outperform a given task better than any classical strategy. As shown in recent years, the unprecedented control and precision provided by ultracold gases in optical lattices makes these systems optimal candidates for such a technology. Furthermore, since the dynamical control over the optical lattice parameters permits the simultaneous coupling between nearest atom-lattice sites, these systems are also increasingly used as quantum simulators to mimic distinct complex condensed matter Hamiltonians [1].

The controlled generation of double well lattices, i.e., lattices whose unit cells contain two sites, has opened the possibility to isolate and address individually pairs of atoms, and hence to manipulate the interactions between them. Seminal results are the demonstration of controlled exchange interaction between pairs of neutral atoms in an optical lattice when the atoms are forced to be in the same location [2], and the demonstration of superexchange interactions [3], showing that the interactions between atoms trapped in two adjacent sites of the optical lattice can be made analogous to the interactions between atomic spins in magnetic materials. While Ref. [2] sets a basis to perform in a controlled manner two qubit gates between neighboring atoms in the double well lattice, Ref. [3] opens a direct path towards the realization of low-temperature quantum magnets and a variety of many-body spin models with ultracold atoms.

The atomic interaction control achieved with optical lattices also has direct applications to quantum computation. A particularly well suited approach that exploits the innate massive parallelism of such systems to perform quantum computation is the measurement based quantum computation (MBQC), where information is processed by means of a sequence of measurements on a highly entangled initial state. It

requires the capability to create a *universal cluster state*, that is, a multipartite quantum state able to reproduce any entangled quantum state in two dimensions, and to perform local single qubits operations. Using as qubits two internal states of atoms in a two-dimensional (2D) optical lattice, it is possible to create a highly entangled quantum state by means of controlled collisions [4], which is indeed a prerequisite for the generation of a universal cluster state.

Although neutral atoms couple weakly to the environment and they have relatively long coherence times compared with the time scale associated with the achievable coupling strength, when atoms are brought to an entangled state decoherence will rapidly destroy any quantum superposition of atoms. The larger the entangled system is, the faster it will decohere. To fight against decoherence one should prepare the atoms in quantum states that are robust against external perturbations. For periodic arrays of double wells [5–7], resilient encoding schemes using two internal states (two Zeeman levels) of the atoms have been proposed. In these schemes, each double well traps two two-level particles to encode a logical qubit. The logical space is spanned by the singlet and triplet states of the two spin-1/2 particles along the quantization axis (here denoted by z), $\{|S\rangle = \frac{1}{\sqrt{2}}(|\uparrow\rangle|\downarrow\rangle - |\downarrow\rangle|\uparrow\rangle)$ and $|T_0\rangle = \frac{1}{\sqrt{2}}(|\uparrow\rangle|\downarrow\rangle + |\downarrow\rangle|\uparrow\rangle)\}$. Since these states have a zero z component of the total spin, such encoding is insensitive to fluctuations of the magnetic field along the quantization axis. In practice, such an encoding scheme is very well suited for robust controlled interactions along one, let us say horizontal, direction. To create a universal 2D cluster state (cluster states in one dimension are not universal), interactions and hence entanglement between neighboring atoms along both the horizontal and the vertical directions should be performed in such a way that robustness is preserved. In the above encoding, interactions along the vertical direction will leave the subspace of zero spin components along the quantization axis, becoming very fragile in front of external magnetic field fluctuations noise. In this paper we
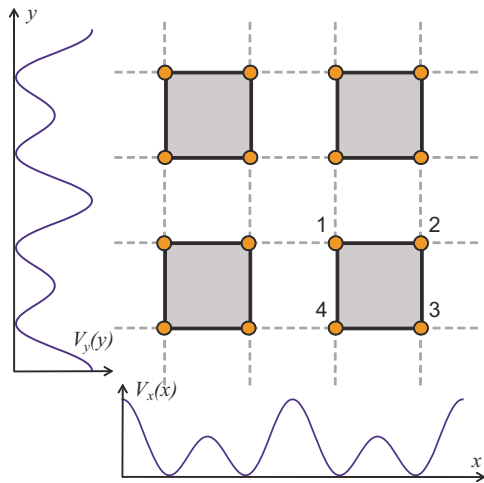
FIG. 1. (Color online) The optical superlattice consists of a periodic array of 2×2 plaquettes. The 2D optical trapping potential is created by adding two superlattice potentials $V_x(x)$ and $V_y(y)$ illustrated in the bottom and left panels. The intraplaquette coupling is represented by the solid lines and the interplaquette coupling is represented by the dashed lines.

show how this limitation can be overcome by using 2D optical superlattices.

In passing, let us point out that superimposing secondary optical lattices (or "superlattices") on top of the primary ones to further modify the potential in which the atoms are trapped permits us in general to create polymerized lattices. By polymerized lattices we mean lattices consisting of weakly coupled groups of neighboring atomic sites denoted as plaquettes. An example of a polymerized lattice is a square lattice made of smaller squares. The intraplaquette interactions in such lattices might be strong and may even be designed to include many(>2)-body terms, while the interplaquette interactions might be much weaker. Polymerized lattices allow us, for instance, to engineer valence bond solids on demand, to study topological spin liquids, and one might envisage them as potential quantum circuits. It is also very appealing to try to use the plaquettes as qubits or qudits (elementary systems with more than two internal states) for quantum information processing and implement quantum logical gates, quantum protocols, and quantum error correction in such systems by employing either interatomic interactions and/or interactions with external (electric, magnetic, laser) fields.

Here we take advantage of the two-dimensional superlattices to present new schemes to prepare universal 2D cluster states using the plaquettes as logical qubits. The superlattices create a periodic array of *plaquettes*, i.e., 2×2 potential wells (as shown in Fig. 1), each of them filled with an atom with two internal degrees of freedom (spin-1/2 particle). On each plaquette, we encode a single logical qubit using the *twofold singlet subspace* of the four 1/2 spins, as shown in Fig. 1. Thus by doubling the physical resources in comparison with the two physical qubit encoding previously mentioned, we obtain the desired encoding that is decoherence free against uniform magnetic field fluctuations in arbitrary directions.

The encoding scheme using the singlet subspace of four qubits has been previously studied for the quantum dot sys-

tems, and it is also called the "supercoherent qubit" [8–10]. Also, it has been shown that in such a configuration, tunable Heisenberg superexchange interactions (between neighboring spins, including the diagonal and off diagonal ones) are sufficient for universal quantum computation [11,12]. In the model we propose here, the generation of a universal cluster state demands (i) the ability to perform one qubit gates to prepare all logical qubits in the initial state $|+\rangle = 1/\sqrt{(2)}[|0\rangle + |1\rangle]$, and (ii) the realization of controlled-phase gates, $U = \mathrm{diag}(1,1,1,-1)$, between nearest logical qubits, i.e., between plaquettes, to create a maximally entangled 2D cluster state. Notice that the superlattice geometry of Fig. 1 does not induce interactions along the diagonals sites on each plaquette, and thus the most challenging ingredient for universality is, indeed, the two qubit (two plaquette) gate. In this paper, we propose three different approaches to couple the logical qubits that either preserve the singlet subspace at the end of the gate operation or keep the state within the singlet subspace even during the whole completion of the gate. In all approaches, we take into account realistic available tools and discuss the practical limitations in optical superlattices. In our first approach, we exploit the additional vibrational mode of the optical trap to facilitate the logical coupling gate. In our second approach, we extend the earlier proposals [9,10] by removing the requirement of equal coupling strengths for all six pairs within the plaquette (more feasible for 2D optical superlattices), while we still obtain the effective Hamiltonian within the logical subspace sufficient for universal gates. In our last approach, we include tunable Ising-type interactions between neighboring spins (attainable with neutral atoms in optical lattices [13]) and use the optimal control techniques to find efficient and robust pulse sequences for the logical coupling gate.

We notice that other proposals which exploit the superlattice structure in two dimensions to create a universal resource (which is different from the universal cluster state) for MBQC by connecting Bell entangled pairs by entangling phase gate have been proposed recently [7].

The paper is organized as follows: first, in Sec. II we present the general ideas for generating cluster states within a decoherence free subspace (DFS) using optical superlattices. Then, in Sec. III we briefly review the singlet DFS of the plaquette and describe operations of a single logical qubit using superexchange couplings. Finally, in Sec. IV we consider the key challenge of implementing the logical controlled-phase gate with the singlet DFS encoding. We propose three interesting approaches for the controlled-phase gate: the geometric phase approach, the perturbative approach, and the optimal control approach. A detailed comparison among the three approaches is summarized at the end of this section (Table I) before we present our conclusion in Sec. V.

II. DECOHERENCE-FREE CLUSTER STATES

One promising approach to quantum computation is the MBQC [14,15], which uses universal resources such as the cluster states. The cluster states can be efficiently prepared by initializing all lattice spins in the product state of $|+\rangle$

TABLE I. Comparison among three approaches. See Sec. IV D for discussion.

	Geometric phase approach	Perturbative approach	Optimal control approach
Time scale for CZ gate	$1/J$	J/J'^2	$1/J$
Duration out of DFS	$1/t$	0	$1/J$
Systematic errors	$(t/U)^2$	$(J'/J)^2$	0
Inhomogeneity errors	$(\delta t/t)^2$, $(\delta\Delta/t)^2$	$(\delta J/J)^2$, $(\delta J'/J')^2$	$(\delta J/J)^2$
Sites per CZ gate	4	8	4
Simultaneous coupling	Yes	Two steps	Yes
Major interactions	Superexchange Single particle tunneling	Superexchange	Superexchange Ising interaction
Superlattice wavelengths	λ, 2λ, 4λ	λ, 2λ, 4λ, $4\lambda/3$	λ, 2λ
Vibrational levels	Ground+excited	Ground	Ground
Physical process	Clear	Clear	Hard to interpret
Control complexity	Medium	Low	High

$=\frac{1}{\sqrt{2}}(|0\rangle+|1\rangle)$ and performing the *controlled-phase gate* between all pairs of neighboring spins. The controlled-phase gate induces an additional factor -1 if both input qubits are in state $|1\rangle$. Up to some individual qubit rotations, the controlled-phase gate can be achieved by Ising-type interaction between two input qubits.

The preparation of a cluster state has been demonstrated using optical lattices [4], with logical qubits directly stored in individual spins. Controlled collisions are used to implement the controlled-phase gate between neighboring spins. However, such atomic qubits for the controlled-collision scheme are vulnerable to magnetic field fluctuations, which limits the practical implementation of the MBQC.

The optical superlattice inducing a periodic array of 2 $\times 2$ plaquettes (as shown in Fig. 1) can be created by superimposing two optical lattice potentials with short and long wavelengths differing by a factor of 2 [16] along both the x and y directions. The effective optical trapping potential becomes

$$V = V_x(x) + V_y(y), \qquad (1)$$

where $V_u = V_{u,s}\cos^2(\frac{2\pi}{\lambda}u-\phi_{u,s}) + V_{u,l}\cos^2(\frac{\pi}{\lambda}u-\phi_{u,l})$ for $u=x,y$. The short-lattice wavelength is λ, and the parameters $V_{u,s}$, $V_{u,l}$, $\phi_{u,s}$, and $\phi_{u,l}$ are controlled by the intensities and phases of the laser beams.

For integer filling with one particle per site, each plaquette has four particles. The four spin-$1/2$ particles have a twofold singlet subspace with total spin zero along all directions (i.e., $S_{tot}=0$). Thus the singlet subspace is the DFS insensitive to uniform magnetic field fluctuations.

The *intraplaquette couplings* (solid lines in Fig. 1) enable operations of the single logical qubit encoded in the plaquette. (Note that by manipulating intraplaquette couplings minimum instances of topological matter can be demonstrated in the same optical superlattice [17].) In order to

create the decoherence-free cluster states, we will also need *interplaquette couplings* (dashed lines in Fig. 1) to implement the controlled-phase gates.

There are eight sites for two neighboring plaquettes. If only four middle sites are involved for the controlled-phase gate (e.g., for the geometric phase approach in Sec. IV A or the optimal control approach in Sec. IV C), it is possible to simultaneously apply controlled-phase gates to couple all horizontal (or vertical) neighboring plaquettes with no overlap of sites involved for different controlled-phase gates as shown in Fig. 2. Meanwhile, if all eight sites from both plaquettes are involved for the controlled-phase gate (e.g.,
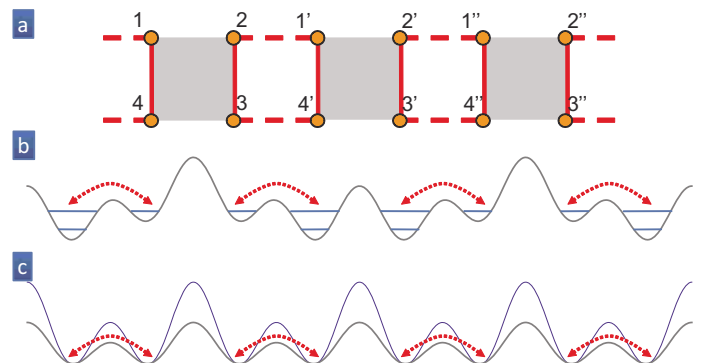

FIG. 2. (Color online) Simultaneous coupling between neighboring plaquettes. (a) It is possible to simultaneously implement the controlled-phase gates between neighboring plaquettes along the horizontal direction, if only four sites are involved for each controlled-phase gate (e.g., for the geometric phase approach or the optimal control approach). (b) The optical superlattice (with interplaquette coupling and alternating energy offset for odd and even plaquettes, created by $\lambda,2\lambda,4\lambda$) can yield the interplaquette coupling for the geometric phase approach. (c) The spin-dependent optical superlattice (indicated by thin and thick lines of potential profiles) can generate Ising interaction [13] useful for the optimal control approach.

the perturbative approach in Sec. IV B), two steps are needed to couple the plaquettes along the horizontal direction: first couple each even plaquette with the neighboring odd plaquette on the left, and then couple each even plaquette with the neighboring odd plaquette on the right.

In order to use the prepared cluster state for the MBQC, we should also be able to measure the individual qubits. This can be achieved by first converting the spin singlet or triplet states into different particle number configurations [2,16], and then using various techniques of coherent optical control with subwavelength resolution [18–20] to projectively count the particle number at a specific site (without compromising the coherence for the remaining sites).

In the next two sections, we will consider the rotation of single logical qubit using intraplaquette couplings, and the controlled-phase gate between two logical qubits using the additional interplaquette couplings, respectively.

III. LOGICAL QUBIT ENCODED IN THE PLAQUETTE

In this section, we focus on the operations within the plaquette via *intraplaquette coupling*. For concreteness, we consider bosonic particles, and similar results can be obtained for fermionic particles as well. The following Hubbard Hamiltonian governs the dynamics of a single plaquette, with spin-independent tunnelings and interactions (we will introduce an additional vibration level in Sec. IV):

$$H = - \sum_{\langle i,j \rangle, \sigma} (t_{ij} a_{i\sigma}^\dagger a_{j\sigma} + \text{H.c.}) + \frac{1}{2} U \sum_i n_i(n_i - 1) + \sum_{i,\sigma} \mu_i n_{i\sigma},$$
(2)

where $a_{i\sigma}$ ($a_{i\sigma}^\dagger$) is the annihilation (creation) operator, $n_{i\sigma}$ is the particle number operator for site $i = 1, \ldots, 4$ with spin $\sigma = \uparrow, \downarrow$, and $n_i = n_{i,\uparrow} + n_{i,\downarrow}$. The tunneling amplitudes ($t_H = t_{12} = t_{34}$ and $t_V = t_{23} = t_{41}$) and the offset energies (μ_i) can be changed by tuning the superlattice parameters. The large onsite interaction $U \gg t_H, t_V$ ensures that the system is in the Mott insulator regime with fixed particle number for each site.

Particle tunneling only occurs virtually between neighboring sites, which leads to the *superexchange coupling*

$$H_{eff} = - J_H (\vec{s}_1 \cdot \vec{s}_2 + \vec{s}_3 \cdot \vec{s}_4) - J_V (\vec{s}_2 \cdot \vec{s}_3 + \vec{s}_4 \cdot \vec{s}_1),$$
(3)

where $\vec{s}_i$ are Pauli operators for the spin at site i. The coupling strengths $J_H = t_H^2/U$ and $J_V = t_V^2/U$ can be changed independently, by tuning the barriers between the sites as illustrated in Fig. 3. Controlling the superexchange couplings is sufficient to perform arbitrary rotations of the logical qubit encoded in the plaquette.

A. Singlet subspace for four spins

The space of four 1/2-spin particles span a subspace of total spin 2, three subspaces of total spin 1 and two subspaces of total spin 0. We use the twofold *singlet subspace* of the plaquette to encode the logical qubit. The singlet subspace is spanned by

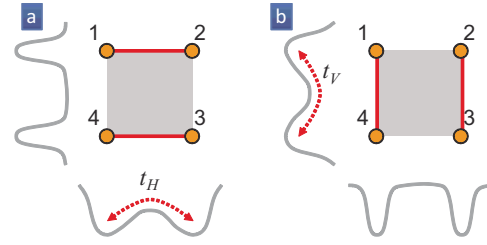$$|\Psi_H\rangle = |S\rangle_{1,2} \otimes |S\rangle_{3,4},$$
(4)

FIG. 3. (Color online) Intraplaquette superexchange couplings. The coupling strengths are (a) $J_H = t_H^2/U$ between horizontal neighbors and (b) $J_V = t_V^2/U$ between vertical neighbors. They can be changed independently by tuning the barriers between the sites.

$$|\Psi_V\rangle = |S\rangle_{2,3} \otimes |S\rangle_{4,1},$$
(5)

with $|S\rangle_{i,j} \equiv \frac{1}{\sqrt{2}}(|\uparrow\rangle_i|\downarrow\rangle_j - |\downarrow\rangle_i|\uparrow\rangle_j)$. $|\Psi_H\rangle$ (or $|\Psi_V\rangle$) is the product state of two singlet pairs along the horizontal (or vertical) direction, which can be prepared using the procedure demonstrated in [3].

The singlet subspace is decoherence free, because it is insensitive to the uniform magnetic field fluctuations. In addition, measuring a single spin will not distinguish the states from singlet subspace, and this is a source of protection against local perturbations. Since $\langle\Psi_H|\Psi_V\rangle = 1/2 \neq 0$, it is more convenient to use the orthogonal states $|0\rangle \equiv |\Psi_V\rangle$ and $|1\rangle \equiv \frac{2}{\sqrt{3}}(\frac{1}{2}|\Psi_V\rangle - |\Psi_H\rangle)$. We can also write the orthogonal states in terms of the singlets and triplets for vertical pairs (2, 3) and (4, 1) [11]:

$$|0\rangle = |S\rangle_{2,3}|S\rangle_{4,1},$$
(6)

$$|1\rangle = \frac{1}{\sqrt{3}}[|T_+\rangle_{2,3}|T_-\rangle_{4,1} - |T_0\rangle_{2,3}|T_0\rangle_{4,1} + |T_-\rangle_{2,3}|T_+\rangle_{4,1}],$$
(7)

where $|T_{+,0,-}\rangle = \{|\uparrow\rangle|\uparrow\rangle, \frac{1}{\sqrt{2}}(|\uparrow\rangle|\downarrow\rangle + |\downarrow\rangle|\uparrow\rangle), |\downarrow\rangle|\downarrow\rangle\}$. For such a choice of basis, the subsystem of two spins (2, 3) is sufficient to determine the logical states $|0\rangle$ and $|1\rangle$, because the corresponding reduced density matrices,

$$\rho_{2,3}^{|0\rangle} = \text{Tr}_{4,1}[|0\rangle\langle 0|] = (|S\rangle\langle S|)_{2,3},$$
(8)

$$\rho_{2,3}^{|1\rangle} = \text{Tr}_{4,1}[|1\rangle\langle 1|] = \frac{1}{3}(|T_+\rangle\langle T_+| + |T_0\rangle\langle T_0| + |T_-\rangle\langle T_-|)_{2,3},$$
(9)

belong to orthogonal (singlet and triplet) subspaces, $\text{Tr}[\rho_{2,3}^{|0\rangle}\rho_{2,3}^{|1\rangle}] = 0$.

The Pauli operators associated with the logical qubit are $\sigma_x \equiv |0\rangle\langle 1| + |1\rangle\langle 0|$, $\sigma_y \equiv i|0\rangle\langle 1| - i|1\rangle\langle 0|$ and $\sigma_z \equiv |0\rangle\langle 0| - |1\rangle\langle 1|$. Within the singlet subspace the logical operator σ_z can be achieved by operating the (2, 3) spins

$$\sigma_z \doteq -\frac{1}{2}(1 + \vec{s}_2 \cdot \vec{s}_3),$$
(10)

where we use "$\doteq$" to represent the special equality valid within the singlet subspace. Since $\vec{s}_2 \cdot \vec{s}_3 \doteq \vec{s}_4 \cdot \vec{s}_1$ (i.e., either both pairs are singlets or both are triplets), σ_z can also be implemented by operating the (4, 1) spins,

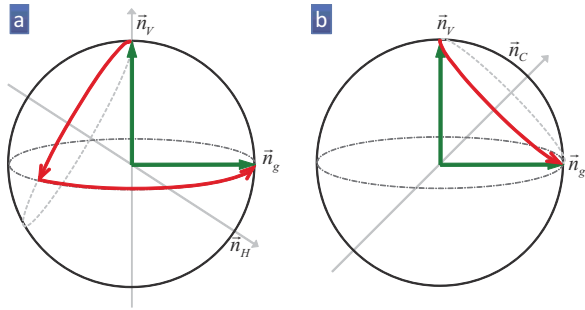$$\sigma_z \doteq -\frac{1}{2}(1 + \vec{s}_4 \cdot \vec{s}_1).$$
(11)

FIG. 4. (Color online) The Bloch sphere representation for the singlet subspace. The state $|0\rangle$ ($|1\rangle$) is associated with the north (south) pole. (a) The superexchange coupling J_H (J_V) is associated with the rotation around the $\vec{n}_H$ ($\vec{n}_V$) axis. Here $\vec{n}_H=(\frac{\sqrt{3}}{2},0,\frac{-1}{2})$ and $\vec{n}_V=(0,0,1)$. The sequential rotations around the $\vec{n}_H$ and $\vec{n}_V$ axes can rotate the Bloch vector from $\vec{n}_V$ to $\vec{n}_g=(\frac{1}{\sqrt{2}},0,\frac{1}{\sqrt{2}})$ [i.e., state $\frac{1}{\sqrt{2}}(|0\rangle+|1\rangle)$]. (b) Alternatively combined superexchange coupling (with contributions from both J_H and J_V) can implement the rotation around the axis $\vec{n}_C$, which rotates the Bloch vector from $\vec{n}_V$ to $\vec{n}_g$ in one step.

B. Rotating logical qubit with superexchange coupling

We now consider arbitrary rotations in the singlet subspace using superexchange couplings. First of all, the superexchange coupling Hamiltonian commutes with the total spin operator of the plaquette $[H_{eff},\vec{s}_1+\vec{s}_2+\vec{s}_3+\vec{s}_4]=0$, due to the identity $[\vec{s}_i\cdot\vec{s}_j,\vec{s}_i+\vec{s}_j]=0$. Consequently, the superexchange coupling preserves the singlet subspace (with zero total spin). Within the singlet subspace we have

$$\vec{n}_H\cdot\vec{\sigma}\doteq\tfrac{1}{2}-\tfrac{1}{4}(\vec{s}_1\cdot\vec{s}_2+\vec{s}_3\cdot\vec{s}_4), \tag{12}$$

$$\vec{n}_V\cdot\vec{\sigma}\doteq\tfrac{1}{2}-\tfrac{1}{4}(\vec{s}_2\cdot\vec{s}_3+\vec{s}_4\cdot\vec{s}_1) \tag{13}$$

with $\vec{n}_H=(\frac{\sqrt{3}}{2},0,\frac{-1}{2})$ and $\vec{n}_V=(0,0,1)$ as illustrated in Fig. 4(a). The constant of $1/2$ can be neglected, as it only induces an overall phase during the evolution. The rotations about these axes can be controlled by switching on/off the superexchange couplings of J_H and J_V, which varies expentially with the height of the corresponding barriers. Since the angle between $\vec{n}_H$ and $\vec{n}_V$ is $2\pi/3$, arbitrary rotation of the Bloch sphere can be achieved within four operations. (This is a special case of the general theorem [21,22] stating that $k+2$ operations are sufficient for arbitrary rotation given the angle η between the two rotation axes satisfies $\frac{\pi}{k}>\min(\eta,\pi-\eta)\geq\frac{\pi}{k+1}$.)

The product state of two vertical singlet pairs $|0\rangle=|\Psi_V\rangle$ can be initialized using the procedure demonstrated in [3]. Universal rotation enables dynamical preparation of arbitrary logical state encoded in singlet subspace. For example, $|+\rangle=\frac{1}{\sqrt{2}}(|0\rangle+|1\rangle)$ can be prepared by two-step evolution $e^{-i\vec{n}_V\cdot\vec{\sigma}\theta_V}e^{-i\vec{n}_H\cdot\vec{\sigma}\theta_H}|\Psi_V\rangle$ with $2\theta_H=2\sin^{-1}\frac{\sqrt{2}}{\sqrt{3}}\approx109.5°$ and $2\theta_V=\pi-\sin^{-1}\frac{\sqrt{2}}{\sqrt{3}}\approx125.3°$, as shown in Fig. 4(a). Alternatively, we can tune the relative strength between $\vec{n}_H\cdot\vec{\sigma}$ and $\vec{n}_V\cdot\vec{\sigma}$ to achieve the total coupling $\vec{n}_C\cdot\vec{\sigma}$ with $\vec{n}_C=(\frac{1}{\sqrt{2}},0,\frac{1}{\sqrt{2}})$, and prepare $|+\rangle$ in one step $e^{-i\vec{n}_C\cdot\vec{\sigma}(\pi/2)}|\Psi_V\rangle$, as illustrated in Fig. 4(b). Note that all the plaquettes can be simultaneously prepared in the $|+\rangle$ state. In order to create the decoherence-free
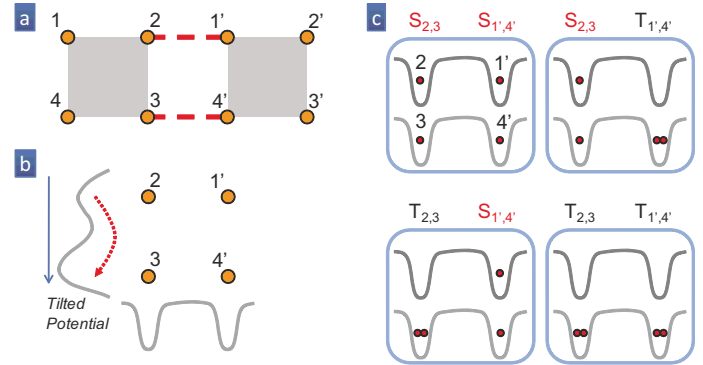

FIG. 5. (Color online) Geometric phase approach to controlled-phase gate (step 1). (a) The sites from two neighboring plaquettes are labeled. (b) The intraplaquette trapping potential along the vertical direction is adiabatically tilted. This results in single (or double) occupancy at the lower site if the vertical pair of particles is in the singlet (or triplet) state. (c) Particle number configurations are plotted for four possible of spin states: $S_{2,3}\otimes S_{1',4'}$, $S_{2,3}\otimes T_{1',4'}$, $T_{2,3}\otimes S_{1',4'}$, and $T_{2,3}\otimes T_{1',4'}$. (S and T indicate singlet and triplet.)

cluster state, we need the controlled-phase gate between the logical qubits encoded in neighboring plaquettes.

IV. CONTROLLED-PHASE GATE

We now consider interplaquette couplings (dashed lines in Fig. 1). In particular, we focus on implementing the controlled-phase gate between two neighboring plaquettes, which induces an additional -1 phase if both encoded qubits are in the logical state $|1\rangle$. In principle, the controlled-phase gate can be achieved by the Ising-type interaction between the logical qubits, but unfortunately such interaction is not immediately available from the lattice experiments, as the effective Ising term $\sigma_z\sigma_z'$ requires four-site interaction $(\vec{s}_2\cdot\vec{s}_3)(\vec{s}_4'\cdot\vec{s}_1')$ [see Eqs. (10) and (11)]. However, since what we want is the specific unitary evolution rather than the interaction, it is actually more feasible to implement the unitary evolution directly.

In the following, we present three different approaches to implement the controlled-phase gate between two neighboring plaquettes. For concreteness, we only consider coupling two neighboring plaquettes along the horizontal direction, while all three approaches can also couple neighboring plaquettes along the vertical direction.

A. Geometric phase approach

The first approach uses the vibration levels and the geometric phase to achieve the controlled-phase gate between neighboring plaquettes [Fig. 5(a)]. The geometric phase is proportional the surface area enclosed by the evolution trajectory in the Bloch sphere (associated with the two energy levels that are degenerate). For example, if a half of the Bloch sphere is enclosed, the system acquires a geometric phase π. We first consider the bosonic particles. It takes three steps to achieve the controlled-phase gate:

Step 1. We lower the interplaquette barrier and adiabatically tilt the intraplaquette potential along the vertical direc-
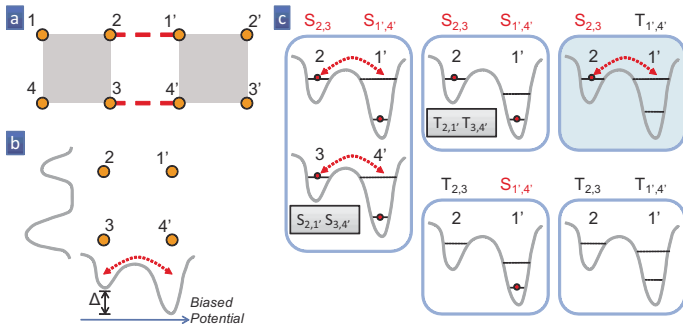
FIG. 6. (Color online) Geometric phase approach to controlled-phase gate (step 2). (a) The sites from two neighboring plaquettes are labeled. (b) A defined bias ($\triangle$) of the interplaquette potential is quickly applied and the interplaquette barrier is lowered to facilitate the resonant tunneling along the horizontal direction. (c) Resonant tunneling (between the vibrational ground level of the left site and the vibrational excited level of the right site) can occur for the following two cases: (i) each of the left and right sites has exactly one particle, and the two particles are in the singlet state (see the left panel), (ii) the left site has one particle and the right site has zero particles (see the highlighted upper right panel). All other configurations are off-resonant, with negligible tunneling. After time $2\pi/t$, a geometric phase π from the resonant tunneling is obtained for $S_{2,3} \otimes T_{1',4'}$ (the highlighted upper right panel), while only a trivial geometric phase (0 or 2π) is obtained for the other three cases ($S_{2,3} \otimes S_{1',4'}$, $T_{2,3} \otimes S_{1',4'}$, and $T_{2,3} \otimes T_{1',4'}$).

tion [Fig. 5(b)]. Each lower site will be occupied by one particle (or two particles) if the vertical pair of particles is in the singlet (or triplet) state [Fig. 5(c)]. For example, if the spins (2, 3) are in the singlet state (denoted as $S_{2,3}$), the transfer of particle from site 2 to site 3 is prevented by the symmetry requirement of bosonic particles, resulting in one particle in site 3 [see the upper two panels in Fig. 5(c)]. If the spins (2, 3) are in the triplet subspace (denoted as $T_{2,3}$), the particle from site 2 is adiabatically transferred to site 3, leaving two particles in site 3 [see the lower two panels in Fig. 5(c)]. Similar spin-dependent transfer also happens to other sites, such as (1', 4').

Step 2. We quickly apply a defined bias to the interplaquette lattice potential and lower the interplaquette barrier along the horizontal direction [Fig. 6(b)]. This induces single particle resonant tunneling with rate t between the vibrational ground state at site 2 and the vibrational excited state at site 1' [33], if there is one particle at site 2 and zero particle at site 1' [see the highlighted upper right panel in Fig. 6(c)]. By waiting for time $2\pi/t$, we obtain the geometric phase π from the resonant tunneling for $S_{2,3} \otimes T_{1',4'}$. As detailed in Sec. IV, for all other three cases ($S_{2,3} \otimes S_{1',4'}$, $T_{2,3} \otimes S_{1',4'}$, and $T_{2,3} \otimes T_{1',4'}$) we only obtain a trivial geometric phase 0 (or 2π).

Step 3. We change the intraplaquette potential to the initial balanced position along the vertical direction (having one particle per site) and restore each plaquette to the logical subspace.

A recent superlattice experiment uses the resonant tunneling and the blockade induced by on-site interaction to count the number of atoms [23]. This experiment demonstrates that the presence or absence of resonant tunneling can be highly

sensitive to the number of particles in the lattice sites. The geometric phase approach can be regarded as an extension that uses the resonant tunneling to coherently imprint a geometric phase for a specific particle number configuration (corresponding to certain logical state).

The procedure for the fermionic particles is almost the same as that for the bosonic particles, except for the following three differences. First, the bias of the energy offset needs to be $\Delta = \omega + U_R^{ab}$ for fermionic particles (whereas $\Delta = \omega$ for bosonic particles), where ω is the vibrational excitation energy and U_R^{ab} is the on-site interaction between ground and excited levels at the right site (1' or 4'). Second, the geometric phase π is obtained from the resonant tunneling associated the subspace $T_{2,3} \otimes S_{1',4'}$ for fermionic particles (whereas it is associated with $S_{2,3} \otimes T_{1',4'}$ for bosonic particles). Third, the geometric phase is 0 for the remaining cases for fermionic particles (whereas it might be either 0 or 2π for bosonic particles).

It is tempting to consider using $\Delta = \omega$ for the fermionic particles, as we might expect that by exchanging the roles of singlet and triplets, the fermionic particles could be mapped to bosonic particles. However, the roles of singlet and triplets are not exactly symmetric. For example, consider the case with one particle per site after step 1. For bosonic particles, the system is in the subspace $S_{2,3} \otimes S_{1',4'}$ that has finite projection to $S_{2,1'} \otimes S_{3,4'}$ and $T_{2,1'} \otimes T_{3,4'}$ (but not $T_{2,1'} \otimes S_{3,4'}$ or $S_{2,1'} \otimes T_{3,4'}$), which yields a trivial 0 or 2π geometric phase. For fermionic particles, the system is in the subspace $T_{2,3} \otimes T_{1',4'}$ that has finite projection to $T_{2,1'} \otimes S_{3,4'}$ and $S_{2,1'} \otimes T_{3,4'}$, as well as $S_{2,1'} \otimes S_{3,4'}$ and $T_{2,1'} \otimes T_{3,4'}$, which thus may yields a nontrivial π geometric phase.

The detailed calculations for both bosonic and fermionic particles are presented in Appendix A.

B. Perturbative approach

The second approach uses both the intra- and interplaquette couplings acting on the eight sites. The intraplaquette coupling induces an energy gap between the logical states (i.e., singlet subspace) and other nonlogical states, while the interplaquette coupling acts as a perturbation that induces different phase shifts for different logical states. The interplaquette coupling can be efficiently achieved using superexchange interaction between the interplaquette neighboring sites.

The key challenge is to obtain the intraplaquette interaction, with finite Heisenberg interaction between the sites along the diagonal and off-diagonal directions. We can overcome the challenge by using a different design of the optical lattice.

1. Lattice geometry and energy levels

We want to obtain the Hamiltonian with intraplaquette interaction:

$$H_{intra} = J \sum_{i=1,2,3,4} \vec{s}_i \cdot \vec{s}_{i+1} + d \sum_{i=1,2} \vec{s}_i \cdot \vec{s}_{i+2}, \quad (14)$$

where the exchange interaction $J = \pm t^2/U$ ($d = \pm \tilde{t}^2/U$) is induced by the tunneling between the nearest neighbors (next-
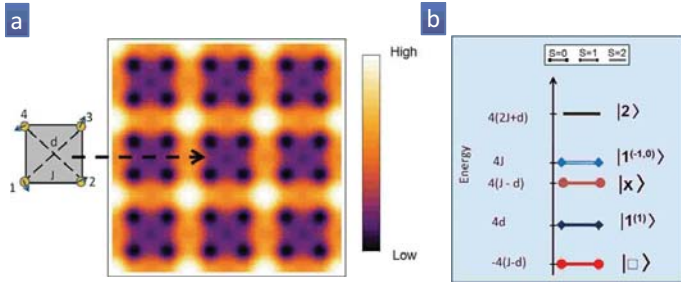
FIG. 7. (Color online) (a) Density plot of the lattice potential [see Eq. (15)], which generates an array of 2×2 plaquettes in the x-y plane with periodicity of $2\pi/k$. Using parameters $V^l=60E_R$, $V^s=9E_r$, and $V'=10E_r$, with E_R and E_r photon recoil energy of the long and short lattices, respectively, one can achieve a parameter regime with $d/J\approx0.2$. (b) Energy levels of a single plaquette described by the Hamiltonian given in Eq. (14). In the plot we assume fermionic atoms, i.e., $J,d>0$ (fermions). For bosons $J,d<0$ the order of the energy levels is the reverse, i.e., the $S=2$ is the lowest energy state.

nearest neighbors) with tunneling rate t ($\tilde{t}$). The positive and negative signs are for fermions and bosons, respectively. To simplify the notation, we have identified $\vec{s}_5$ with $\vec{s}_1$. Such a type of interaction can be created by a lattice potential of the form [see Fig. 7(a)]

$$V(x,y,z) = V^c(x,y) + V_x^s(x) + V_y^s(y), \quad (15)$$

where $V_u^s(u)=\frac{V^s}{2}\cos(2ku)-\frac{V^l}{2}\cos(ku)$ are the typical double well superlattice formed by the superposition of two independent sinusoidal potentials which differ in periodicity, $a=\pi/k,2\pi/k$, by a factor of 2 [3] and $V^c(x,y)=-V'^2(k(x-y))\cos^2[k(x+y)]$ is an additional potential that allows us to control the diagonal couplings within the plaquettes. It can be constructed, for example, from a folded, retroreflected beam with out-of-the-plane polarization [24]. By varying the depths of the short V^s and V^l long lattices it is possible to control the intra- and interplaquette coupling independently, and in particular to make the latter negligibly small and the plaquettes independent.

As the intensity of the nonseparable part of the potential is ramped up, a minima at the center of the plaquettes develops. If the strength of the latter is such that the energies of bound states in this minima are larger than the energies of the lowest vibrational states at the plaquette sites it is possible to tune the ratio $\tilde{t}/t$ without populating the central site, which is required for the validity of Eq. (14). For example, using the parameters $V^l=60E_R=15E_r$, $V^s=9E_r$, and $V'=10E_r$, with $E_R=\hbar^2k^2/(8m)$ and $E_r=\hbar^2k^2/(2m)$ the photon recoil energy of the long and short lattices, respectively, one can achieve a parameter regime with $\tilde{t}/t\approx0.5$ with an energy gap to the first vibrational state in the central well of order $E_g/t\approx10$. It is very difficult to increase $\tilde{t}/t$ close to 1 by just controlling the lattice potential, because the energy gap disappears and the central sites become accessible. Therefore we will focus on the case $d<J$.

The eigenstates associated with Eq. (14) can be classified according with their total spin S. As shown in Fig. 7(b), there are two singlet ($S=0$) states,

$$|\square\rangle = \frac{1}{\sqrt{3}}(|\Psi_H\rangle + |\Psi_V\rangle), \quad (16)$$

$$|\times\rangle = |\Psi_H\rangle - |\Psi_V\rangle, \quad (17)$$

with energies $E(|\square\rangle)=-4(J-d)$ and $E(|\times\rangle)=+4(J-d)$, respectively. There are three $S=1$ states denoted by $|1^{(-1,0,1)}\rangle$, with energies $E(1^{(q)})=4J$, $4J$, and $4d$, respectively. For fermionic (bosonic) atoms the highest (lowest) energy state is a $S=2$ state, $|2\rangle$ with energy $E(2)=4(2J+d)$.

We want to use the singlet states within each plaquette as encoded qubits and perform a phase gate between them by coupling nearest-neighbor plaquettes into a "superplaquette" (i.e., 2×4 potential wells). A superplaquette can be achieve by superimposing laser beams with periodicities 4λ and $4\lambda/3$ along one axis [25]. Such wavelengths are experimentally available for typical alkali-metal atoms or can be engineered by intersecting pairs of laser beams at appropriated angles [26]. The 4λ isolates pairs of adjacent plaquettes along one direction and the extra $4\lambda/3$ lattice is needed to balance the offset created when the latter lattice is added. When pairs of plaquettes are weakly coupled into a superplaquette the Hamiltonian that connects the plaquettes is given by

$$H_c = J'(\vec{s}_2 \cdot \vec{s}_{1'} + \vec{s}_3 \cdot \vec{s}_{4'}). \quad (18)$$

We want to use the coupling to implement a controlled-phase gate between the singlet eigenstates in the two plaquettes. To achieve that we require that the interplaquette coupling is weak [i.e., $J'\ll\min\{4d,8(J-d),4(J-2d)\}$] and derive an effective Hamiltonian by adiabatically eliminating the all $S>0$ states.

In the following we discuss the implementation of the controlled-phase gate for the experimentally relevant regime $d<J$. (The ideal case of $d=J$ is discussed in Appendix B.)

2. Perturbative approach with $d<J$

For the 2D plaquette implementation the diagonal coupling d is always smaller than J and therefore the singlet states within the plaquette are nondegenerate,

$$|\Delta E| = |E(|\times\rangle) - E(|\square\rangle)| = 8|J-d| > 0. \quad (19)$$

Regardless of this issue, it is still possible to derive an effective Hamiltonian provided that the interplaquette coupling J' is less than the energy difference between $|\times\rangle$ and all other states [see Fig. 7(b)]:

$$J' \ll \min\{4d,8(J-d),4(J-2d)\}. \quad (20)$$

From this consideration we observe that close to $d=0,J/2$, and J, the perturbative approach (based on $|\square\rangle$ and $|\times\rangle$) breaks down and we should stay away from these points.

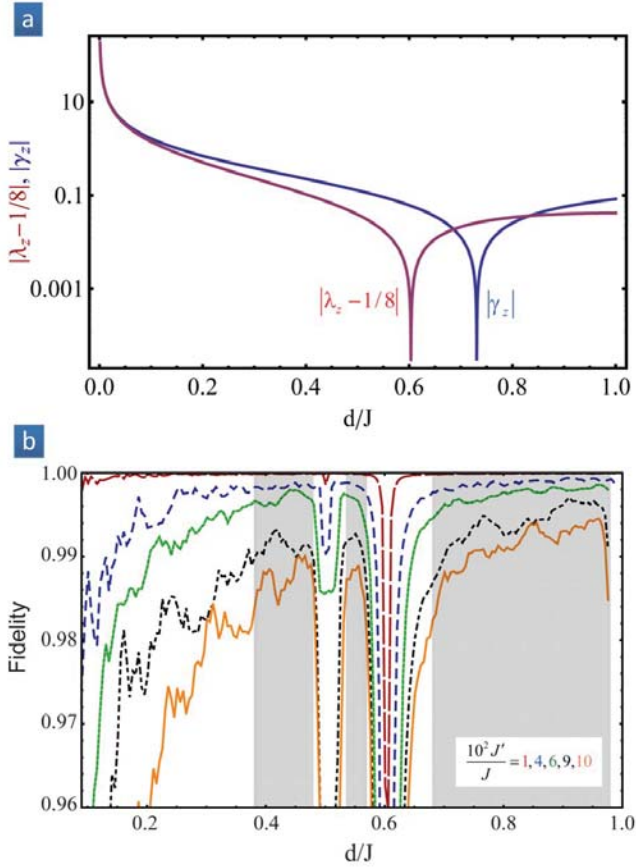As detailed in Appendix B, we can obtain the effective Hamiltonian

FIG. 8. (Color online) (a) Parameters of the effective Hamiltonian for the general case $d \neq J$. At the point $d \approx 0.62J$, the Ising term in the effective Hamiltonian vanishes, $\lambda_z = \frac{1}{8}$ (see text). (b) The controlled-phase gate fidelity F on a superplaquette as a function of d/J for different rations of J'/J. For same d/J, the smaller J'/J the higher the fidelity. There are four critical points at which the fidelity drops considerably; these are $d/J \approx 0, 0.5, 0.62, 1$. At $d/J \approx 0$ and 0.5, one of the singlet states becomes degenerate with one $S=1$ state and consequently the effective Hamiltonian breaks down. At the $d/J \approx 0.62$ the Ising term vanishes and at $d=J$ the rotating wave approximation used in the simplification of the effective Hamiltonian becomes invalid. The shadow regions are the ones where the achievable fidelity is higher than 0.98.

$$H_{i,i+1}^{eff} = \left(\frac{\Delta E}{2} - \frac{J'^2 \gamma_z}{J} \right) \sum_{j=i,i+1} \hat{\sigma}_j^z$$
$$- \frac{J'^2}{J} \left[\frac{1}{8} \hat{\vec{\sigma}}_i \cdot \hat{\vec{\sigma}}_{i+1} + \left(\lambda_z - \frac{1}{8} \right) \hat{\sigma}_i^z \hat{\sigma}_{i+1}^z \right], \quad (21)$$

where $\hat{\sigma}$ are effective Pauli matrices acting on the $|\square\rangle$, $|\times\rangle$ states, and

$$\lambda_z = \frac{1}{48} \left(\frac{9J}{d} - \frac{8J}{d-3J} + 2 - \frac{24J}{d+J} + \frac{J}{2J-d} \right), \quad (22)$$

$$\gamma_z = \frac{1}{48} \left(\frac{9J}{d} + \frac{8J}{d-3J} - 8 - \frac{J}{2J-d} \right). \quad (23)$$

In Fig. 8(a) the parameters λ_z and γ_z are plotted as a function of d/J.

Within a superplaquette the term $\hat{\vec{\sigma}}_i \cdot \hat{\vec{\sigma}}_{i+1}$ commutes with $H_{i,i+1}^{eff}$ (it only introduces a phase $\phi_T = \frac{J'^2}{\hbar J 8} t_c$ in the effective triplet subspace: $|\square,\square\rangle$, $|\times,\times\rangle$, and $(|\square,\times\rangle + |\times,\square\rangle)/\sqrt{2}$ and $\phi_S = -\frac{3J'^2}{\hbar J 8} t_c$ for the effective singlet states: $(|\square,\times\rangle - |\times,\square\rangle)/\sqrt{2}$). Here t_c stands for the duration of the controlled-phase gate, i.e., $\frac{J'^2}{J} t_c (\lambda_z - \frac{1}{8}) = \hbar(2n-1)\pi/4$, with an integer $n=1,2,\ldots$. Consequently $H_{i,i+1}^{eff}$ can be used to perform a controlled-phase gate within a superplaquette. We use the standard echo technique (i.e., π pulses at $t_c/2$ and t_c for each of the encoded qubits) to remove the unwanted $\hat{\sigma}_j^z$ term from the effective Hamiltonian in Eq. (21). The controlled-phase gate can be achieved by the unitary evolution

$$U = X e^{-i(H_{intra}+H_c)t_c/2} X e^{-i(H_{intra}+H_c)t_c/2}, \quad (24)$$

where X represents the echo π pulses for the encoded qubits, which can be achieved via intraplaquette superexchange couplings.

We use the exact diagonalization to calculate the controlled-phase gate fidelity $F = |f|^2$ with

$$f = \frac{1}{N} \text{Tr}[U_{c-phase}^\dagger P U P], \quad (25)$$

where P is the projection operator to the singlet subspace for each plaquette. In Fig. 8(b), we plot F as a function of d/J for different rations of J'/J, with $n=1$. The figure shows that at the points $d \approx 0.5J$, $d \approx 0.62J$, $d=0$, $d=J$ there is an abrupt drop of the fidelity, as the ratio J'/J is increased. The drop at these points is expected since at $d \approx 0.5J$ and $d \approx 0$ one of the singlet states becomes degenerate with one $S=1$ and consequently the effective Hamiltonian breaks down. At $d \approx 0.62J$, $\lambda_z = 1/8$ [see Fig. 8(a)] the Ising term vanishes and at $d=J$ the two singlets become degenerate and the rotating wave approximation (assumed for the derivation of the effective Hamiltonian in Appendix B) is no longer justified.

Away from these points the derived effective Hamiltonian provides a good description of the dynamics and for values of $J' \approx 0.1J$ one can get a gate fidelity above 0.98. In the plot we highlight with a gray shadow the d/J parameter regime where the achievable fidelity is above 0.98. However, among these shadow regions only the regime $d/J < 0.5$ is experimentally achievable using the lattice geometry described early in this section. The small fluctuations in the fidelity curves are due to the nonenergy preserving terms neglected to obtain the effective Hamiltonian (see Appendix B), which can be suppressed when $J' \ll \sqrt{8(J-d)J}$.

The Heisenberg term $\hat{\vec{\sigma}}_i \cdot \hat{\vec{\sigma}}_{i+1}$, on the other hand, does not commute with $H_{i+1,i+2}^{eff}$ and consequently the phase gate cannot be applied simultaneously to all plaquettes. Instead it has to be applied first between the superplaquettes formed by the plaquettes $2i+1$, $2i+2$ and subsequently between the superplaquettes formed from plaquettes $2i+2$, $2i+3$ (see Fig. 9). Additionally, in order to create a cluster state across all the plaquette array, it is required to fine tune the parameters and time evolution to eliminate the different phase accumulated by the triplet and singlet states in the encoded spin basis due to the Heisenberg term at t_c. Consequently, for multipartite
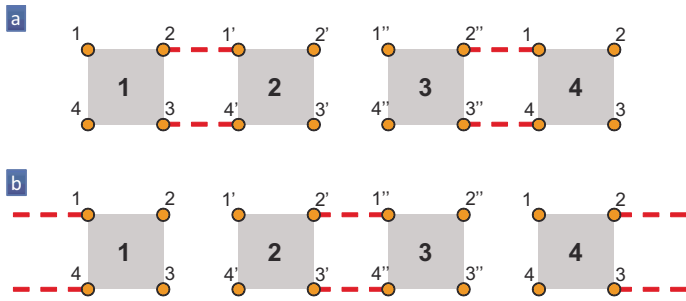
FIG. 9. (Color online) For the $d < J$, the cluster state generation has to be applied in two steps (a) and (b).

entanglement generation not all d/J values are allowed but only the ones which satisfy the following conditions:

$$\phi_T - \phi_S = 2\pi m, \tag{26}$$

$$\frac{J'^2}{J} t_c \left(\lambda_z - \frac{1}{8} \right) = \hbar(2n-1) \frac{\pi}{4}, \tag{27}$$

where n and m are integers. In Fig. 10(a), we show a set of allowed d/J values which satisfy the conditions given by Eq. (26), for different n and m values. Here we also highlight with a gray shadow the corresponding d/J values which yield a fidelity higher than 0.98 for $J'/J < 0.1$. In Fig. 10(b) we show two examples of traces of the phase gate fidelity vs J'/J: $(n, m) = (1, 1), (3, 4)$ [indicated in panel (a) by a square] computed by exact diagonalization of the superplaquette
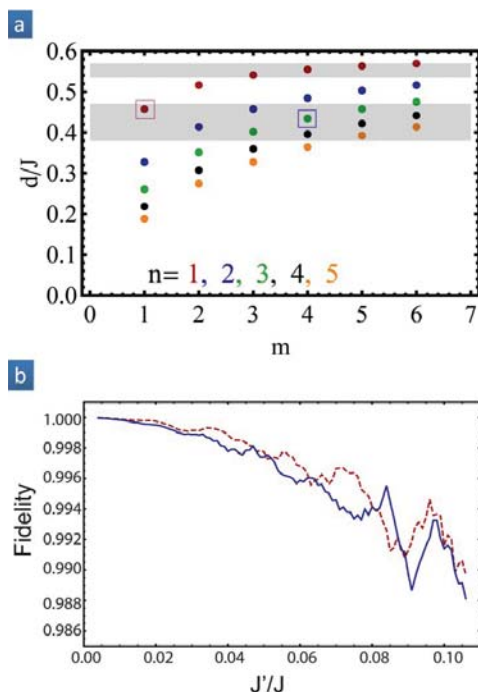

FIG. 10. (Color online) Examples of controlled-phase gate with the perturbative approach. (a) The values of d/J that satisfy the conditions stated in Eqs. (26). The shadow regions highlight the regime where the phase gate fidelity can be larger than 0.98 for $J'/J < 0.1$. (b) The controlled-phase gate fidelity F as a function of J'/J can be calculated by exact numerical diagonalization. The red dashed (or blue solid) curve is for $(n, m) = (1, 1)$ [or (3, 4)], which is also indicated by the red (blue) square in panel (a).

Hamiltonian. The figure shows that it is always possible to find parameters which allow for a high gate fidelity. However, here we are only including errors due to higher order terms neglected in the derivation of the effective Hamiltonian. In realistic experiments other external errors such as lattice inhomogeneities are always present, which can be minimized at the expense of a larger J'/J ratio (faster evolution). There is consequently a tradeoff between faster time evolution and small perturbative corrections.

In conclusion, we have presented a scheme to perform controlled-phase gates in the encoded singlet subspace. This perturbative scheme has two advantages: (i) the plaquettes are always in the decoherence free subspace; (ii) it is easy to implement as it only relays on the coherent dynamical evolution without further manipulations. Due to the fact that the dynamics is determined by a second order effective Hamiltonian the achievable fidelity with the proposed schemes can become very high but at the cost of slower time evolution. If the strongly interacting regime is reached by using a Feshbach resonance, one can achieve values of J of order of 100 Hz and therefore cluster generation times of order $0.1 - 1$ s. These generation times are slow but longer than the encoded qubits' decoherence time due to their insensitivity against environmental decoherence [3].

C. Optimal control approach

We now consider the optimal control approach to fast, high fidelity implementation of the controlled-phase gate [between the horizontal neighboring plaquettes (1, 2, 3, 4) and $(1', 2', 3', 4')$ as shown in Fig. 5(a)]. The key challenge here is to identify an efficient set of operators that (i) enable the unitary evolution of the controlled-phase gate, and (ii) are feasible using optical superlattices as well. We first provide a set of operators sufficient to achieve the controlled-phase gate with arbitrary precision. After that we numerically find the pulse sequences for these operators to implement the controlled-phase gate.

1. Choice of operators

In principle, tunable Heisenberg superexchange interactions are sufficient for the controlled-phase gate by coupling all eight sites [11]. However, for the optical lattice experiments, we would like to achieve the controlled-phase gate by coupling as few sites as possible, preferably using global rotations for all spins and Heisenberg or Ising interactions between neighboring sites [3,13].

According to Eqs. (10) and (11), we need at least two sites from each plaquette to determine the σ_z operator. Since the controlled-phase gate depends on both σ_z operators from the plaquettes, we should consider at least four sites to implement the controlled-phase gate. It turns out that coupling the four middle sites $(2, 3, 4', 1')$ is sufficient to achieve the controlled-phase gate, which significantly reduces the complexity compared with the earlier proposal that couples all eight sites [11].

We consider the Hamiltonian

$$H(t) = \sum_{k=1}^{5} \alpha_k(t) O_k, \tag{28}$$

where $\{\alpha_k(t)\}$ are the time-dependent control variables for the set of operators

$$O_1 = \vec{s}_2 \cdot \vec{s}_3, \tag{29}$$

$$O_2 = \vec{s}_1' \cdot \vec{s}_4', \tag{30}$$

$$O_3 = s_{2,z} s_{1,z}' + s_{3,z} s_{4,z}', \tag{31}$$

$$O_4 = s_{2,x} + s_{3,x} + s_{1,x}' + s_{4,x}', \tag{32}$$

$$O_5 = s_{2,y} + s_{3,y} + s_{1,y}' + s_{4,y}'. \tag{33}$$

To justify that $H(t)$ can implement the controlled-phase gate

$$U_{\text{c-phase}} = \exp\left[-i\frac{\pi}{4}(1-\sigma_z)(1-\sigma_z')\right], \tag{34}$$

we show that $(1-\sigma_z)(1-\sigma_z')$ belongs to the Lie algebra generated by $\{O_k\}_{k=1,\ldots,5}$. We start with these five operators as the *available set* (AS), and calculate the commutators among the AS operators. We then expand the AS by adding new commutators that are not linear combinations of the AS operators. We denote the number of linearly independent AS operators as the dimension of the AS. We repeat the process of calculating the commutators and expanding the AS, until its dimension does not increase any more. We use MATH-EMATICA to iterate the process of expanding the AS until it saturates at dimension 80 (including the identity operator that commutes with all other operators). Finally, we verify that $(1-\sigma_z)(1-\sigma_z') \sim (\vec{s}_2 \cdot \vec{s}_3)(\vec{s}_1' \cdot \vec{s}_4')$ is a linear combination of the AS operators. Therefore according to the local properties from the Lie algebra the set of operators $\{O_k\}_{k=1,\ldots,5}$ is sufficient to implement the controlled-phase gate. The remaining task is to find the solution for $\{\alpha_k(t)\}$.

2. Smooth pulses

We use an algorithm which can be interpreted as a continuous version of the gradient ascent pulse engineering (GRAPE) [27,28], though it is developed in an independent way [29]. The algorithm based on optimal quantum control is summarized in Appendix C. Comparing with the GRAPE method it has the advantage that we can find solutions with specific boundary conditions (e.g., pulses start and end at zero) and in terms of smooth (finite slope) functions of time as well.

More specifically, the particular form of the coefficients $\{\alpha_k(t)\}$ are chosen to be finite sums of sinusoidal functions,

$$\alpha_k(t, x_{k1}, \ldots, x_{kL}) = \sum_{l=1}^{L} x_{kl} \sin\left(\frac{l\pi t}{T}\right), \tag{35}$$

each of which depends on L parameters $\{x_{kl}\}$ ($l=1,\ldots,L$). As mentioned before, note that they fulfill the convenient property that $\alpha_k(0) = \alpha_k(T) = 0$ and that they have a finite slope. Hence we need to optimize $K \times L$ (with $K=5$ operators in our case) parameters x_{kl} which maximize the fidelity $F = |f|^2$, where

$$f = \frac{1}{N}\text{Tr}[U_{\text{c-phase}}^\dagger U(T;x)] = \frac{1}{N}\sum_{n=1}^{N} \langle \psi_n | U_{\text{c-phase}}^\dagger U(T;x) | \psi_n \rangle, \tag{36}$$

for a particular subspace of N states $\{|\psi_n\rangle\}$ ($n=1,\ldots,N$) of dimension $d \geq N$.

In Fig. 11(a) we show an example of pulses obtained with $L=20$, which can attain very low infidelity $\varepsilon = 1-F$, less than 10^{-7} (the value can be further reduced by improving the precision of the numerics). In Fig. 11(b) we plot the infidelity ε as a function of the *relative deviation* $\delta J/J$. We assume that the couplings in Eq. (28) are deviated from α_k to $(1-\delta J/J)\alpha_k$; that is, the system evolves under the deviated Hamiltonian $(1-\delta J/J)H$. For simplicity, we consider the case that $\delta J/J$ is time independent. (For example, imperfect calibration of barrier height or barrier thickness may induce such proportional, time-independent deviation in superexchange couplings.) We find that the infidelity remains a constant value (approximately 10^{-7}) for very small deviations (with $\delta J/J < 10^{-4}$), while the infidelity scales as $(\delta J/J)^2$ for larger deviations (with $\delta J/J > 10^{-3}$) which is also plotted using the linear scale in Fig. 11(c). Such quadratic dependence to the deviation is not uncommon, as the infidelity for single spin rotations also scales quadratically with the deviation. The quadratic dependence can be regarded as a direct consequence of the optimization procedure, which finds a local minimum of the function with first order derivatives being zero.

3. Experimental implementation

We now briefly discuss the implementation of operators $\{O_k\}_{k=1,\ldots,5}$ (and $\{O_k\}$) for the cluster state preparation. The operators of O_1 and O_2 can be achieved by superexchange interaction using superlattice techniques [3], while the operator of O_3 can be obtained from spin-dependent tunneling in optical lattices [13]. Furthermore, we note that the evolution of the Ising interactions O_3 between all horizontal neighboring plaquettes can be performed simultaneously, because they act on different groups of physical spins as illustrated in Fig. 2. For the same reason, the operators of O_4 and O_5 can be performed simultaneously for all spins by driving the entire optical lattice with appropriate microwave pulses [4]. Therefore the simultaneous controlled-phase gates between all horizontally neighboring plaquettes can be achieved.

D. Comparing three approaches

We compare the three approaches (see Table I) in the following aspects: (i) two relevant time scales: the time to implement the controlled-phase gate, and the duration for the plaquette not being protected by the DFS (which should be short compared to the coherence time outside the DFS [34]), (ii) two types of errors contributing to the controlled-Z (CZ) gate infidelity: the systematic errors from the approximations used in our analysis, and the inhomogeneity errors due to the fact that the couplings (e.g., t, Δ, J, and J') are not exactly the same for all plaquettes, (iii) the number of sites involved for each controlled-phase gate: if each gate only couples four
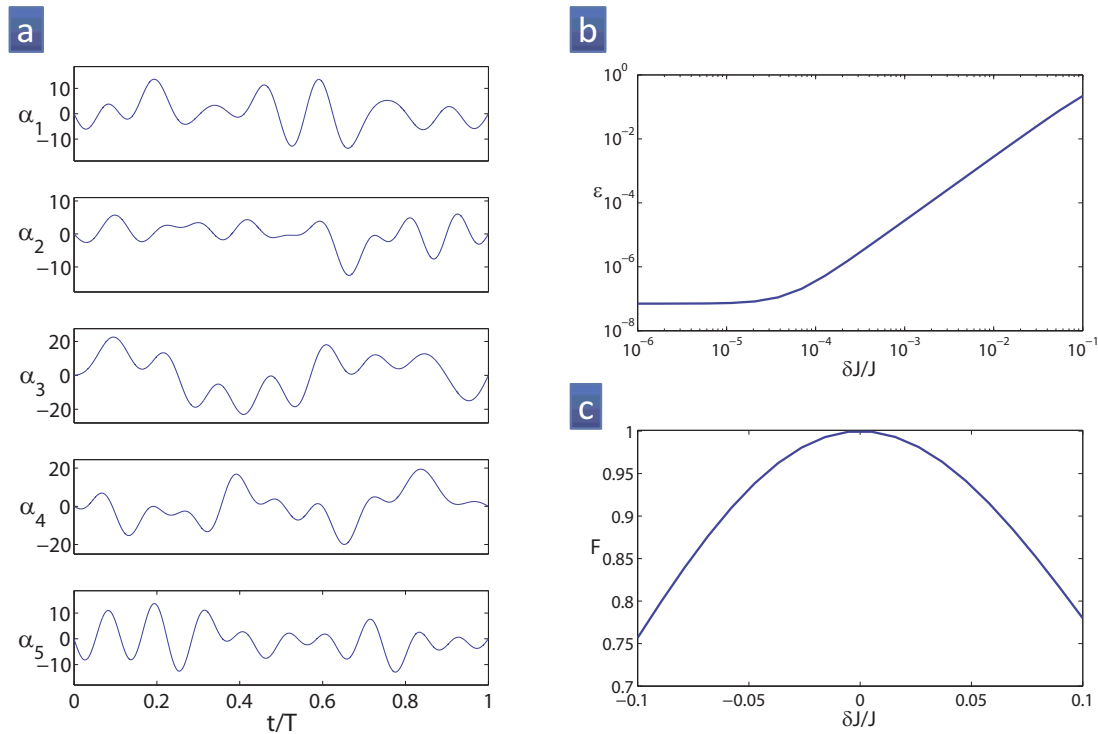
FIG. 11. (Color online) (a) Smooth pulses with $L=20$ yielding to infidelities smaller than 10^{-7}. (b) Infidelity $\epsilon=1-F$ vs the deviation $\delta J/J$ for the smooth pulses. The infidelity is constant at 10^{-7} for $\delta J/J < 10^{-4}$ and increases quadratically with $\delta J/J$ for $\delta J/J > 10^{-3}$. (c) Quadratic dependence of the fidelity with $\delta J/J$.

sites, the controlled-phase gates between all horizontal (or vertical) neighbors can be achieved simultaneously; otherwise two sequential steps are needed, (iv) the major interactions, such as singlet particle tunneling [16], (Heisenberg) superexchange coupling [3], and Ising interaction [13], (v) the wavelength components needed to construct the superlattices, (vi) the relevant vibrational levels, (vii) the interpretation of the physical process, and (viii) the control complexity for time-dependent parameters.

The maximum achievable fidelity for the CZ gate is limited by the systematic and inhomogeneity errors. For the geometric phase approach, the systematic error $(t/U)^2$ is due to the off-resonant tunneling, which is analyzed in Tables II and III for bosonic and fermonic particles, respectively; such off-resonant tunneling can be suppressed by using Feshbach resonances to increase U while keeping the same tunneling rate t. For the perturbative approach, the controlled-phase

gate fidelity is $F > 0.98$ for $J'/J < 0.1$ (Fig. 10). For the optimal control approach, the systematic error is only limited by the precision of the numerics [Figs. 11(b) and 11(c)]. We note that it is important to suppress the inhomogeneity errors, as all three approaches are sensitive to such imperfections. Replacing the parabolic trap with the flat-bottom trap [30] can be one possible solution to reduce the inhomogeneity errors. It would also be interesting to consider other approaches that are insensitive to the inhomogeneity errors.

Overall, the geometric phase approach has the advantage of fast operational time, short unprotected duration, and compatibility of simultaneous coupling. The perturbative approach has the advantage of always being protected by the DFS and favorable control complexity. The optimal control approach has the advantage of fast operational time, vanishing systematic errors, and compatibility of simultaneous coupling.

TABLE II. Energy difference associated with bosonic particle tunneling (δE_1) for various initial number configurations (n_L, n_R^a) and the final total spin at the right site j_R. The bias is set to be $\Delta = \omega$. The resonance condition $\delta E_1 = 0$ is fulfilled for both cases: $(n_L, n_R^a, j_R) = (1, 0, 1/2)$ and $(n_L, n_R^a, j_R) = (1, 1, 0)$.

(n_L, n_R^a)	$j_R = (n_R^a - 1)/2$	$j_R = (n_R^a + 1)/2$
(1, 0)		**0**
(1, 1)	**0**	$-2U_R^{ab}$
(1, 2)	$-U_R^{ab}$	$-4U_R^{ab}$
(2, 1)	$2U_L^{aa}$	$-2U_R^{ab} + 2U_L^{aa}$
(2, 2)	$-U_R^{ab} + 2U_L^{aa}$	$-4U_R^{ab} + 2U_L^{aa}$

TABLE III. Energy difference associated with fermonic particle tunneling (δE_1) for different initial number configurations. The bias is set to be $\Delta = \omega + U_R^{ab}$. For $(n_L, n_R^a) = (1, 1)$, the energy difference is $\mp U_R^{ab}$ for singlet and triplet states, respectively. The resonance condition $\delta E_1 = 0$ is fulfilled only if $(n_L, n_R^a) = (1, 2)$.

(n_L, n_R^a)	δE_1
(1, 0)	U_R^{ab}
(1, 1)	$\mp U_R^{ab}$
(1, 2)	**0**
(2, 1)	$-\frac{1}{2}U_R^{ab} + U_L^{aa}$
(2, 2)	$-U_R^{ab} + U_L^{aa}$

V. CONCLUSION

In conclusion, we have discussed the preparation of large cluster states for neutral atoms in optical superlattices. Each logical qubit is encoded in the decoherence-free singlet subspace of four spins from the 2×2 plaquette, so that it is insensitive to uniform magnetic field fluctuations along an arbitrary direction. Besides arbitrary rotations of single logical qubits achieved by superexchange interaction, we provide three different approaches to couple the logical qubits from neighboring plaquettes, with their properties summarized in Table I. These approaches may also be applied to other quantum systems, such as quantum dots or Josephson junction arrays.

APPENDIX A: GEOMETRIC PHASE APPROACH

1. Geometric phase approach with bosonic particles

We now justify the claim that the geometric phase π is obtained for $S_{2,3} \otimes T_{1',4'}$, while a trivial geometric phase 0 (or 2π) is obtained for the other three cases ($S_{2,3} \otimes S_{1',4'}$, $T_{2,3} \otimes S_{1',4'}$, and $T_{2,3} \otimes T_{1',4'}$). This evolution implements the controlled-phase gate up to a bit-flip of the logical qubit from the left plaquette.

We start by generalizing the on-site interaction Hamiltonian for site i that governs both the ground and excited vibrational levels (denoted as a and b, respectively),

$$H_i = \mu_i n_i + \omega_i n_i^b + \frac{1}{2} U_i^{aa} n_i^a (n_i^a - 1) + \frac{1}{2} U_i^{bb} n_i^b (n_i^b - 1)$$
$$+ U_i^{ab} \left(n_i^a n_i^b + \sum_{\sigma,\sigma'} a_{i,\sigma}^\dagger b_{i,\sigma'}^\dagger b_{i,\sigma} a_{i,\sigma'} \right.$$
$$\left. + \sum_{\sigma,\sigma'} b_{i,\sigma}^\dagger b_{i,\sigma'}^\dagger a_{i,\sigma} a_{i,\sigma'} \right), \tag{A1}$$

where μ_i is the energy offset, ω_i is the vibrational frequency, $U_i^{\alpha\beta}$ is the on-site interaction strength between levels α and β for site i. The particle number operators are $n_i^a = \sum_\sigma a_{i,\sigma}^\dagger a_{i,\sigma}$, $n_i^b = \sum_\sigma b_{i,\sigma}^\dagger b_{i,\sigma}$, and $n_i = n_i^a + n_i^b$. Given large vibrational frequency $\omega_i \gg U_i^{ab}$, we may safely neglect those energy nonconserving terms $\sum_{\sigma,\sigma'} b_{i,\sigma}^\dagger b_{i,\sigma'}^\dagger a_{i,\sigma} a_{i,\sigma'}$.

For the biased potential between the two horizontal sites (L and R) (as shown in Fig. 12), we consider one vibrational level for the left site and two levels for the right site:
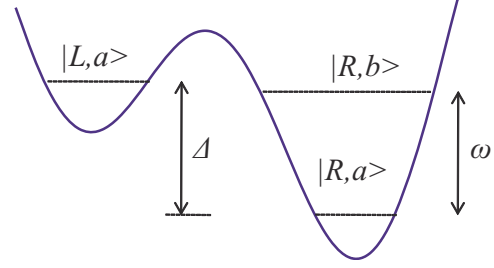

FIG. 12. (Color online) The biased potential for the sites L and R. The vibrational ground levels are $|L,a\rangle$ and $|R,a\rangle$, with energy difference $\triangle$. The vibrational excited level for the right site is $|R,b\rangle$ with excitation energy ω.

$$H_L = \Delta n_L + U_L^{aa} n_L (n_L - 1), \tag{A2}$$

$$H_R = \omega_R n_R^b + \frac{1}{2} U_R^{aa} n_R^a (n_R^a - 1) + \frac{1}{2} U_R^{bb} n_R^b (n_R^b - 1)$$
$$+ U_R^{ab} \left[2 n_R^a n_R^b + \vec{J}_R^2 - \frac{n_R^a + n_R^b}{2} \left(\frac{n_R^a + n_R^b}{2} + 1 \right) \right], \tag{A3}$$

where $\Delta = \mu_L - \mu_R$ is the bias in the potential (i.e., energy difference between the ground levels for the two sites), and $\vec{J}_R$ is the total spin for the right site (see Appendix A 2 for detailed derivation).

Given quantum numbers (n_L, n_R^a, n_R^b, j_R), the on-site energies are

$$E_L[n_L] = \Delta n_L + U_L^{aa} n_L (n_L - 1), \tag{A4}$$

$$E_R[n_R^a, n_R^b, j_R] = \omega_R n_R^b + \frac{1}{2} U_R^{aa} n_R^a (n_R^a - 1) + \frac{1}{2} U_R^{bb} n_R^b (n_R^b - 1)$$
$$+ U_R^{ab} f[n_R^a, n_R^b, j_R], \tag{A5}$$

where

$$f[n_R^a, n_R^b, j_R] = 2 n_R^a n_R^b - \frac{n_R^a + n_R^b}{2} \left(\frac{n_R^a + n_R^b}{2} + 1 \right) + j_R(j_R + 1) \tag{A6}$$

for $[(n_R^a + n_R^b)/2] \geq j_R \geq [(n_R^a - n_R^b)/2]$. Note that $n_R^b = 0$ implies $f[n_R^a, 0, j_R = n_R^a/2] = 0$. For $n_R^b = 1$, we have $f[n_R^a, 1, j_R = (n_R^a + 1)/2] = 2 n_R^a$ and $f[n_R^a, 1, j_R = (n_R^a - 1)/2] = n_R^a - 1$ [35]. Thus the energy difference for the bosonic particle tunneling from the left site to the right site is

$$\delta E_1[n_L, n_R^a, j_R] = E_L[n_L] + E_R[n_R^a, 0, n_R^a/2]$$
$$- E_L[n_L - 1] - E_R[n_R^a, 1, j_R]$$
$$= (\Delta - \omega) + U_L^{aa}(n_L - 1) - U_R^{ab} f[n_R^a, 1, j_R]. \tag{A7}$$

In Table II, we list the energy difference associated with bosonic particle tunneling with $\Delta = \omega$. There are two possibilities to fulfill the condition of resonant tunneling. The first case is $(n_L, n_R^a, j_R) = (1, 0, 1/2)$. This corresponds to the resonant tunneling between the sites $(2, 1')$ in the highlighted upper right panel $S_{2,3} \otimes T_{1',4'}$ of Fig. 6(c), yielding a geomet-

ric phase π. The second case is $(n_L, n_R^a, j_R) = (1, 1, 0)$. This corresponds to resonant tunneling for both pairs of sites $(2, 1')$ and $(3, 4')$ as shown in the left panel of Fig. 6(c), yielding a trivial geometric phase 2π. The remaining cases are off-resonant $|\delta E_1| \gg t$, which yields a trivial geometric phase 0. Therefore we obtain a nontrivial geometric phase π only for $S_{2,3} \otimes T_{1',4'}$.

2. On-site interaction for bosonic particles

We now derive Eq. (A3) from Eq. (A1). The key step is to simplify the exchange term $\Sigma_{\sigma,\sigma'} a_{i,\sigma}^\dagger b_{i,\sigma'}^\dagger b_{i,\sigma} a_{i,\sigma'}$ using the particle number operators and the total spin operator. For clarify, we drop the subindex i (or R).

Use the Schwinger representation, we define the spin operator $\vec{J}^a$ for the ground vibrational level

$$J_x^a = \tfrac{1}{2}(a_\uparrow^\dagger a_\downarrow + a_\downarrow^\dagger a_\uparrow), \tag{A8}$$

$$J_y^a = \frac{1}{2i}(a_\uparrow^\dagger a_\downarrow - a_\downarrow^\dagger a_\uparrow), \tag{A9}$$

$$J_z^a = \tfrac{1}{2}(n_\uparrow^a - n_\downarrow^a), \tag{A10}$$

$$j^a = \frac{1}{2}(n_\uparrow^a + n_\downarrow^a) = \frac{n^a}{2}, \tag{A11}$$

with $(\vec{J}^a)^2 = j^a(j^a+1)$. Similar definition for $\vec{J}^b$ can be introduced for the excited vibrational level. Thus the total spin is $\vec{J} = \vec{J}^a + \vec{J}^b$.

We may rewrite the exchange interaction as

$$\sum_{\sigma,\sigma'} a_{i,\sigma}^\dagger b_{i,\sigma'}^\dagger b_{i,\sigma} a_{i,\sigma'} \tag{A12}$$

$$= \sum_\sigma a_{i,\sigma}^\dagger a_{i,\sigma} b_{i,\sigma}^\dagger b_{i,\sigma} + \sum_\sigma a_{i,\sigma}^\dagger a_{i,\bar{\sigma}} b_{i,\bar{\sigma}}^\dagger b_{i,\sigma} \tag{A13}$$

$$= (2j^a j^b + 2J_z^a J_z^b) + 2(J_x^a J_x^b + J_y^a J_y^b) \tag{A14}$$

$$= 4j^a j^b + \vec{J}^2 - (j^a + j^b)(j^a + j^b + 1) \tag{A15}$$

$$= n^a n^b + \vec{J}^2 - \frac{n^a + n^b}{2}\left(\frac{n^a + n^b}{2} + 1\right). \tag{A16}$$

Plugging the above expression into Eq. (A1) gives us Eq. (A3).

3. Geometric phase approach with fermionic particles

The procedure for the fermionic particles is almost the same as that for the bosonic particles, except for the following three differences. First, the bias of the energy offset needs to be $\Delta = \omega + U_R^{ab}$ for fermionic particles (whereas $\Delta = \omega$ for bosonic particles). Second, the geometric phase π is obtained from the resonant tunneling associated the subspace $T_{2,3} \otimes S_{1',4'}$ for fermionic particles (whereas it is associated

with $S_{2,3} \otimes T_{1',4'}$ for bosonic particles). Third, the geometric phase is 0 for the remaining cases for fermionic particles (whereas it might be either 0 or 2π for bosonic particles).

For fermionic particles, the on-site interaction Hamiltonian for site i that governs both the ground and excited vibrational levels (a and b) is

$$H_i = \mu_i n_i + \omega_i n_i^b + U_i^{aa} n_{i,\uparrow}^a n_{i,\downarrow}^a + U_i^{bb} n_{i,\uparrow}^b n_{i,\downarrow}^b$$
$$+ U_i^{ab}\left(n_i^a n_i^b - \sum_{\sigma,\sigma'} a_{i,\sigma}^\dagger b_{i,\sigma'}^\dagger b_{i,\sigma} a_{i,\sigma'}\right), \tag{A17}$$

where we have safely neglected the energy nonconserving terms $\Sigma_{\sigma,\sigma'} b_{i,\sigma}^\dagger b_{i,\sigma'}^\dagger a_{i,\sigma} a_{i,\sigma'}$ for $\omega_i \gg U_i^{ab}$.

For the biased potential between the two horizontal sites (L and R) as shown in Fig. 12, we have

$$H_L = \Delta n_L + U_L^{aa} n_{L,\uparrow} n_{L,\downarrow}, \tag{A18}$$

$$H_R = \omega n_R^b + U_R^{aa} n_{R,\uparrow}^a n_{R,\downarrow}^a + U_R^{bb} n_{R,\uparrow}^b n_{R,\downarrow}^b$$
$$+ U_R^{ab}\left(n_R^a n_R^b - \sum_\sigma n_{R,\sigma}^a n_{R,\sigma}^b - \sum_\sigma a_\sigma^\dagger a_{\bar{\sigma}} b_{\bar{\sigma}}^\dagger b_\sigma\right). \tag{A19}$$

Given quantum numbers (n_L, n_R^a, n_R^b, j_R), we obtain the on-site energy

$$E_L[n_L] = \Delta n_L + U_L^{aa} \delta_{n_L,2}, \tag{A20}$$

$$E_R[n_R^a, n_R^b, j_R] = \omega n_R^b + U_R^{aa} \delta_{n_R^a,2} + U_R^{bb} \delta_{n_R^b,2}$$
$$+ \tfrac{1}{2}\tfrac{1}{2} U_R^{ab}(n_R^a n_R^b + \eta_{n_R^a,n_R^b,j_R}), \tag{A21}$$

where

$$\eta_{n_R^a, n_R^b, j_R} = (3 - 4j_R) \delta_{n_R^a,1} \delta_{n_R^b,1} \tag{A22}$$

for the spin dependent interaction. If $n_R^a = n_R^b = 1$, $\eta = 3$ for spin singlet and $\eta = -1$ for spin triplet states; otherwise, $\eta = 0$.

The energy difference associated with fermionic particle tunneling from the left to the right site is

$$\delta E_1[n_L, n_R^a, j_R] \equiv E_L[n_L] + E_R\left[n_R^a, 0, \frac{1}{2}\delta_{n_R^a,1}\right]$$
$$- E_L[n_L - 1] - E_R[n_R^a, 1, j_R]$$
$$= \left(\Delta - \omega - \frac{1}{2}U_R^{ab}(n_R^a + \eta_{n_R^a,1,j_R})\right) + U_L^{aa} \delta_{n_L,2}. \tag{A23}$$

By choosing $\Delta = \omega + U_R^{ab}$, we fulfill the resonance condition $\delta E_1 = 0$ for $(n_L, n_R^a) = (1, 2)$. In Table III, we list the energy difference associated with fermionic particle tunneling for various particle number configurations.

Here are some remarks on the geometric phase approach. It is crucial to have large and sufficiently different on-site interactions compared with the tunneling rate t, because the virtual tunneling process may induce higher order systematic errors $\sim (t/U)^2$ in the accumulated phase. One may use Feshbach resonances to enhance the on-site interaction and suppress such errors. In addition, the tunneling rate t and the

energy difference Δ should be as homogeneous as possible, since inhomogeneities δt and $\delta\Delta$ may induce leakage errors out of the logical subspace with probability $\sim(\frac{\delta t}{t})^2$ and $(\frac{\delta\Delta}{t})^2$, respectively. Optical lattices in flat-bottom traps [30] may efficiently eliminate such inhomogeneity errors.

APPENDIX B: PERTURBATIVE APPROACH

1. Effective Hamiltonian with *d=J*

For $J=d$ (which might be achieved by placing an additional atom at the center of the plaquette to block its occupancy due to interatomic repulsion [31]), the singlets are degenerated and isolated by an energy gap $4J$ from the threefold degenerate $S=1$ states. Since they are degenerate we can choose any linear combination of them as a basis. For convenience we choose the states $|0\rangle$ and $|1\rangle$ as our basis. These two states can be regarded as the two components of an effective pseudo-spin-1/2 system.

In the absence of any coupling the singlet subspace of the chain is spanned by product states of the effective pseudospin states $|0\rangle$, $|1\rangle$ at the plaquettes and all four possible configurations are degenerate. A finite J' breaks the degeneracy. Since the H_c Hamiltonian does not directly couple the effective pseudospins, they get only coupled through second order virtual processes to intermediate high energy states with $S>0$. Denoting the left and right plaquettes as i and $i+1$, the effective Hamiltonian is given by

$$H_{i,i+1}^{eff} = \sum_{S,S',q,q'} \frac{H_c|S_i^{q(S)}S_{i+1}^{'q'(S')}\rangle\langle S_i^{(q)}S_{i+1}^{'(q')}|H_c}{2E(0)-E(S)-E(S')}. \quad (B1)$$

Here $q(S)$ labels the number of states within a plaquette with total spin S. After some algebra one obtains that

$$H_{i,i+1}^{eff} = -\frac{J'^2}{3J}\left[\tilde{\sigma}_R^z\tilde{\sigma}_L^z - \frac{1}{2}(\tilde{\sigma}_R^z+\tilde{\sigma}_L^z)\right], \quad (B2)$$

where $\tilde{\sigma}_R^z$ are effective Pauli matrices acting on the pseudospin states $|0\rangle$, $|1\rangle$. H^{eff} is an effective Ising Hamiltonian and up to single logical qubit rotations it can be used to generate cluster states encoded with the singlet basis. Since $H_{i,i+1}^{eff}$ commutes with $H_{i+1,i+2}^{eff}$, the cluster state generation can be performed simultaneously in the 2D array of plaquettes.

2. Effective Hamiltonian with *d<J*

For $d<J$, we shall use the eigenbasis $|\square\rangle$ and $|\times\rangle$. We obtain the effective Hamiltonian using the second order perturbation theory:

$$H_{i,i+1}^{eff} = \left(\frac{\Delta E}{2}-\frac{J'^2\gamma_z}{J}\right)\sum_{j=i,i+1}\hat{\sigma}_j^z - \frac{J'^2}{J}\left[\frac{1}{4}\hat{\sigma}_i^x\hat{\sigma}_{i+1}^x + \lambda_z\hat{\sigma}_i^z\hat{\sigma}_{i+1}^z\right]$$

$$-\frac{J'^2}{J}\left[-\frac{1}{4\sqrt{3}}(\hat{\sigma}_i^x\hat{\sigma}_{i+1}^z+\hat{\sigma}_i^z\hat{\sigma}_{i+1}^x) + \frac{1}{4\sqrt{3}}\sum_{j=i,i+1}\hat{\sigma}_j^x\right],$$

$$(B3)$$

where $\hat{\sigma}$ are effective Pauli matrices acting on the $|\square\rangle$, $|\times\rangle$ states, and

$$\lambda_z = \frac{1}{48}\left(\frac{9J}{d}-\frac{8J}{d-3J}+2-\frac{24J}{d+J}+\frac{J}{2J-d}\right), \quad (B4)$$

$$\gamma_z = \frac{1}{48}\left(\frac{9J}{d}+\frac{8J}{d-3J}-8-\frac{J}{2J-d}\right). \quad (B5)$$

In Fig. 8(a) the parameters λ_z and γ_z are plotted as a function of d/J.

The above Hamiltonian is more complex than the one derived for the previous $J=d$ case, however, if the interplaquette coupling is smaller than the energy splitting between the two singlet states, $J'^2/J\ll\Delta E$, it is energetically costly to flip an encoded spin and only the terms that preserve the total effective magnetization are relevant. Consequently, in this regime one can use an effective rotating wave approximation which consists of neglecting the non-energy-preserving terms [last line in Eq. (B3)]. It leads to a simpler effective Hamiltonian:

$$H_{i,i+1}^{eff} = \left(\frac{\Delta E}{2}-\frac{J'^2\gamma_z}{J}\right)\sum_{j=i,i+1}\hat{\sigma}_j^z$$

$$-\frac{J'^2}{J}\left[\frac{1}{8}\hat{\vec{\sigma}}_i\cdot\hat{\vec{\sigma}}_{i+1} + \left(\lambda_z-\frac{1}{8}\right)\hat{\sigma}_i^z\hat{\sigma}_{i+1}^z\right]. \quad (B6)$$

APPENDIX C: OPTIMAL QUANTUM CONTROL WITH SMOOTH PULSES

Here we present the algorithm used to optimize the smooth functions α_k. This algorithm is significantly different from the standard approach in optimal quantum control based on a Lagrangian formulation [28], and is an extension of the one used by some of the authors in [29].

Let us consider that we have the Hamiltonian

$$H(t;x) = \sum_{k=1}^{K}\alpha_k(t,x_{k1},\ldots,x_{kL})O_k = \sum_{k=1}^{K}O_k\sum_{l=1}^{L}x_{kl}J_l(t),$$

$$(C1)$$

where in our case $K=5$ and $J_l(t)=\sin(lt\pi/T)$. We have defined $x\equiv\{x_{kl}\}$ as the set of $K\times L$ parameters that we wish to optimize. The optimization is made such that the unitary evolution operator $U(T;x)$,

$$i\frac{d}{dt}U(t;x) = H(t;x)U(t;x), \quad (C2)$$

with initial condition $U(0;x)=\mathbb{I}$ gets as close as possible to a desired unitary gate U_g acting on a subspace $\{|\psi_n\rangle\}$ of N states of dimension $d\geq N$. This can be quantified with the fidelity

$$f = \frac{1}{N}\text{Tr}[U_g^\dagger U(T;x)] = \frac{1}{N}\sum_{n=1}^{N}\langle\psi_n|U_g^\dagger U(T;x)|\psi_n\rangle.$$

To avoid complex numbers one can use either $F=\text{Re}\{f\}$ or $F=|f|^2$. For simplicity we will derive the algorithm using $F=\text{Re}\{f\}$ (but we have presented the results with $F=|f|^2$ as this

is not sensible to irrelevant global phases). To maximize F we need to compute the derivative of F with respect to the parameters x, i.e., $\partial F/\partial x_{kl}$. If this can be done efficiently, then one can use any of the multiple optimization algorithms which compute the optimal control. In particular, the derivative and the formulas derived below are fed to MATLAB's nonlinear optimization toolbox [32].

The partial derivatives of F can be expressed as

$$\frac{\partial F}{\partial x_{kl}} = \frac{1}{N} \operatorname{Re} \sum_{n=1}^{N} \langle \psi_n | U_g^\dagger \frac{\partial}{\partial x_{kl}} U(T;x) | \psi_n \rangle,$$

which relates the gradient of F to a derivative of the unitary operator $U(T;x)$. Using second-order perturbation theory (see the Appendix in [29] for details) the derivative of $U(T;x)$ can be expressed as

$$\frac{\partial}{\partial x_{kl}} U(t;x) = -iU(t;x)\int_0^t d\tau U(\tau;x)^\dagger \frac{\partial H(\tau;x)}{\partial x} U(\tau;x).$$
(C3)

Hence we get the following closed formula for the gradient of the fidelity:

$$\frac{\partial F}{\partial x_{kl}} = \frac{1}{N} \operatorname{Im} \sum_{n=1}^{N} \int_0^T d\tau \langle \psi_n | U_g^\dagger U(T) U(\tau)^\dagger \frac{\partial H(\tau)}{\partial x_{kl}} U(\tau) | \psi_n \rangle$$
(C4)

(hereafter we omit the x dependence of U and H in order to ease the notation). Though we have a closed formula, we still need to perform the integral. To do so, we devise an efficient procedure which is based on solving three sets of ordinary differential equations (ODEs). First note that the integral in Eq. (C4) can be transformed into $N \times K \times L$ ODEs,

$$\frac{d}{dt}\mathfrak{f}_{nkl}(t) = \frac{1}{N} \operatorname{Im}\langle \psi_n | U_g^\dagger U(T) U(t)^\dagger \frac{\partial H(t)}{\partial x_{kl}} U(t) | \psi_n \rangle, \quad \text{(C5)}$$

with initial conditions $\mathfrak{f}_{nkl}(0)=0$. Thus we have that

$$\frac{\partial F}{\partial x_{kl}} = \sum_{n=1}^{N} \mathfrak{f}_{nkl}(T).$$
(C6)

Then, the algorithm to obtain the gradient of the fidelity, which is fed to MATLAB's non-linear optimization toolbox [32], is given by the following:

(i) Solve the N ODEs,

$$i\frac{d}{dt}|\xi_n(t)\rangle = H(t)|\xi_n(t)\rangle,$$
(C7)

with initial condition $|\xi_n(T)\rangle = U_g|\psi_n\rangle$ and moving backwards in time from T to t.

(ii) Solve the $2N$ ODEs,

$$i\frac{d}{dt}|\psi_n(t)\rangle := H(t)|\psi_n(t)\rangle,$$
(C8a)

$$i\frac{d}{dt}|\xi_n(t)\rangle := H(t)|\xi_n(t)\rangle;$$
(C8b)

with the initial conditions $|\psi_n(0)\rangle = |\psi_n\rangle$, and $|\xi_n(0)\rangle = U(T)^\dagger U_g |\psi_n\rangle$ computed before.

(iii) Solve the $K \times L$ ODEs,

$$\frac{d}{dt}\widetilde{\mathfrak{f}}_{kl} = \frac{J_l(t)}{N}\sum_{n=1}^{N} \operatorname{Im}\langle \xi_n(t)|O_k|\psi_n(t)\rangle,$$
(C9)

with initial condition $\widetilde{\mathfrak{f}}_{kl}(0)=0$. We have defined $\widetilde{\mathfrak{f}}_{kl}=\Sigma_n\mathfrak{f}_{nkl}$ and we have used the expression of the particular Hamiltonian of Eq. (C1). This step can be done simultaneously with step (ii) so that $|\psi_n(t)\rangle$ and $|\xi_n(t)\rangle$ need not be stored.

(iv) The derivatives of the fidelity are then given by

$$\frac{\partial F}{\partial x_{kl}} = \widetilde{\mathfrak{f}}_{kl}(T).$$
(C10)

[1] I. Bloch, Nature (London) **453**, 1016 (2008).

[2] M. Anderlini, P. J. Lee, B. L. Brown, J. Sebby-Strabley, W. D. Phillips, and J. V. Porto, Nature (London) **448**, 452 (2007).

[3] S. Trotzky, P. Cheinet, S. Folling, M. Feld, U. Schnorrberger, A. M. Rey, A. Polkovnikov, E. A. Demler, M. D. Lukin, and I. Bloch, Science **319**, 295 (2008).

[4] O. Mandel, M. Greiner, A. Widera, T. Rom, T. W. Hansch, and I. Bloch, Nature (London) **425**, 937 (2003).

[5] M. S. Tame, M. Paternostro, and M. S. Kim, New J. Phys. **9**, 201 (2007).

[6] A. M. Rey, L. Jiang, and M. D. Lukin, Phys. Rev. A **76**, 053617 (2007).

[7] B. Vaucher, A. Nunnenkamp, and D. Jaksch, New J. Phys. **10**, 023005 (2008).

[8] D. Bacon, K. R. Brown, and K. B. Whaley, Phys. Rev. Lett. **87**, 247902 (2001).

[9] Y. S. Weinstein, C. S. Hellberg, and J. Levy, Phys. Rev. A **72**, 020304(R) (2005).

[10] Y. S. Weinstein and C. S. Hellberg, Phys. Rev. Lett. **98**, 110501 (2007).

[11] D. Bacon, J. Kempe, D. A. Lidar, and K. B. Whaley, Phys. Rev. Lett. **85**, 1758 (2000).

[12] D. P. DiVincenzo, D. Bacon, J. Kempe, G. Burkard, and K. B. Whaley, Nature (London) **408**, 339 (2000).

[13] L. M. Duan, E. Demler, and M. D. Lukin, Phys. Rev. Lett. **91**, 090402 (2003).

[14] R. Raussendorf and H. J. Briegel, Phys. Rev. Lett. **86**, 5188 (2001).

[15] H. J. Briegel and R. Raussendorf, Phys. Rev. Lett. **86**, 910 (2001).

[16] S. Folling, S. Trotzky, P. Cheinet, M. Feld, R. Saers, A. Widera, T. Muller, and I. Bloch, Nature (London) **448**, 1029

(2007).

[17] B. Paredes and I. Bloch, Phys. Rev. A **77**, 023603 (2008).

[18] C. Zhang, S. L. Rolston, and S. Das Sarma, Phys. Rev. A **74**, 042316 (2006).

[19] J. Cho, Phys. Rev. Lett. **99**, 020502 (2007).

[20] A. V. Gorshkov, L. Jiang, M. Greiner, P. Zoller, and M. D. Lukin, Phys. Rev. Lett. **100**, 093005 (2008).

[21] F. Lowenthal, Rocky Mt. J. Math. **1**, 575 (1971).

[22] N. Khaneja, Phys. Rev. A **76**, 032326 (2007).

[23] P. Cheinet, S. Trotzky, M. Feld, U. Schnorrberger, M. Moreno-Cardoner, S. Foelling, and I. Bloch, Phys. Rev. Lett. **101**, 090404 (2008).

[24] J. Sebby-Strabley, M. Anderlini, P. S. Jessen, and J. V. Porto, Phys. Rev. A **73**, 033605 (2006).

[25] A. M. Rey, R. Sensarma, S. Foelling, M. Greiner, E. Demler, and M. D. Lukin, e-print arXiv:cond-mat/0806.0166.

[26] S. Peil, J. V. Porto, B. Laburthe Tolra, J. M. Obrecht, B. E. King, M. Subbotin, S. L. Rolston, and W. D. Phillips, Phys. Rev. A **67**, 051603(R) (2003).

[27] N. Khaneja, T. Reiss, C. Kehlet, T. Schulte-Herbruggen, and S. J. Glaser, J. Magn. Reson. **172**, 296 (2005).

[28] J. Werschnik and E. K. U. Gross, J. Phys. B **40**, R175 (2007).

[29] O. Romero-Isart and J. J. Garcia-Ripoll, Phys. Rev. A **76**, 052304 (2007).

[30] E. Gershnabel, N. Katz, E. Rowen, and N. Davidson, New J. Phys. **6**, 127 (2004).

[31] H. P. Buchler, M. Hermele, S. D. Huber, M. P. A. Fisher, and P. Zoller, Phys. Rev. Lett. **95**, 040402 (2005).

[32] M. A. Branch, T. F. Coleman, and Y. Y. Li, SIAM J. Sci. Comput. (USA) **21**, 1 (1999).

[33] In general, the tunneling rate between two sites in different vibrational bands is zero for an untilted lattice. However, here we have a finite rate t because the Wannier orbitals are distorted for the tilted lattice.

[34] The optimal control algorithm can also minimize the errors accumulated when the system is outside the DFS during the optimal controlled evolution.

[35] The energy difference for the co-tunneling from the left to the right site is $\delta E_2[n_L=2, n_R^a, j_R] = E_L[2] + E_R[n_R^a, 0] - E_L[0] - E_R[n_R^a, 2] = 2(\Delta - \omega) + (U_L^{aa} - U_R^{bb}) - U_R^{ab} f[n_R^a, 2, j_R]$, with $f[n_R^a, 2, j_R=(n_R^a+2)/2] = 4n_R^a$, $f[n_R^a, 2, j_R=\frac{n_R^a}{2}] = 3n_R^a - 1$, and $f[n_R^a, 2, j_R=(n_R^a-2)/2] = 2n_R^a$.